Experimental Study of Time-dependent Failure of High Strain Composites

Kanthasamy Ubamanyu,* Armanj D. Hasanyan,† and Sergio Pellegrino‡
California Institute of Technology, Pasadena, CA, 91125, USA

High strain composites for coilable space structures can undergo micro-structural changes in the time period between stowage and deployment. These changes include the accumulation of residual stresses in response to curvature changes (stress-relaxation) and accumulation of damage, which may lead to rupture of high strain composites. Currently, the mechanisms that cause damage growth and failure are not well understood. In this study, new experimental approaches are explored for applying constant curvature changes, that replicate the stowage conditions while imaging the evaluation of cracks on the compression surface and of damage in the micro-structure of the test sample. The test temperature is raised to accelerate the failure process.

I. Nomenclature

a_T	=	time-shift factor
E_a	=	activation energy
G	=	shear modulus of composite
R	=	universal gas constant
T_0	=	reference temperature
T	=	actual temperature
t	=	real time
t'	=	reduced time
σ_c	=	critical compressive stress
ϕ_0	=	initial fiber misalignment
γ_y	=	yield shear strain of composite
κ_o	=	imposed curvature
κ_f	=	instantaneous failure curvature
κ_o	=	normalized curvature

II. Introduction

High strain composites (HSC) are finding an increasing number of applications in deployable space structures for their low areal density and high stiffness. These remarkable properties are due to the small thickness, on the order of 17.5 µm of the prepregs used for these composites. One of the most prominent areas of application of HSC is in replacing traditionally metallic booms. A HSC thin shell can be tightly coiled around a cylindrical mandrel in order to achieve a high packaging efficiency. As a result, HSC thin shells are considered a cost-effective means of deploying booms for solar arrays, antennas, and other space structures.

A recent application of composite booms was in the deployment of the Roll-Out Solar Array (ROSA) in 2017 [1] on the International Space Station. A deployable spacecraft for the Space Solar Power Project (SSPP) is currently under development at Caltech. This spacecraft is stowed in a coiled form and is deployed to acts as a stiff, lightweight support for functional tiles that generate electricity from sunlight and transmit it as RF electromagnetic waves to

*Graduate Student, Graduate Aerospace Laboratories, 1200 E California Blvd, MC 105-50, Pasadena. e-mail: ubamanyu@caltech.edu

†Postdoctoral Researcher, Graduate Aerospace Laboratories, 1200 E California Blvd, MC 105-50, Pasadena. AIAA Member. e-mail: armanj@caltech.edu

‡Joyce and Kent Kresa Professor of Aerospace and Civil Engineering, Graduate Aerospace Laboratories, 1200 E California Blvd, MC 105-50, Pasadena. AIAA Fellow. e-mail: sergiop@caltech.edu

Earth [2]. A challenge in further extending the application of HSC to space applications is the lack of standardized methods to characterize the damage and failure of these structures. This includes the lack of reliable testing methods for time-dependent failure including viscoelastic and/or viscoplastic behavior, and eventual failure due to rupture.

These effects are especially crucial for HSC, which can be held stowed for a long period of time. In the stowed configuration, flexural strain energy is stored in the structure. In the time period between stowage and deployment, residual stresses accumulate in the structure due to stress-relaxation of the polymer matrix, which may influence the performance of the structure once it is deployed. After a long stowage time, the deployment energy and achievable shape precision of the deployed structure may be impacted [3]. Time-dependent viscoelastic effects on deployment and shape recovery of a composite structure are discussed in [4, 5].

Recent experiments have characterized viscoelastic effects in HSC at the constitutive level. The main challenges in developing constitutive models are that; first due to compliance of HSC laminates it is difficult to apply a constant curvature or uniform bending moments. Second, the need to reduce the time-scale of the tests while still capturing the actual stowage time of a real structure. A notable experimental work in this area is the development of a Column Bending Test method for Long-Term testing (CBT-LT) by Roccor [6, 7], which is a generalization of the earlier Column Bending Test [8] for applying an almost uniform curvature to a test sample for quasi-static testing. In [6] the CBT-LT fixture was modified to allow removal from the loading frame, to be placed in an elevated temperature setting for accelerated testing. The fixtures were periodically put back on the loading frame for in-situ force measurements. This experimental setup addressed the issue of applying a constant curvature and also allowed for in-situ measurements of the stress-relaxation, until rupture. With the in-situ measurements, a Prony series curve fit was used to represent the time-dependent constitutive relation of the test samples.

An earlier test method, the Diametric Compression Test (DCT) was also developed by Roccor, where the test samples are manufactured in the form of cylindrical tubes and compressed using two diametrically opposed plates. Relaxation and rupture were studied by holding the plates at a particular distance apart, with the cylindrical sample compressed. Similar to the CBT-LT, the plates were removed from the load frame during the test, and later placed on the load frame to measure the relaxed stiffness. According to [6], this test can measure strain energy, viscoelastic behavior and inelastic creep of a tubular structure.

These important advances by Roccor in long term testing of HSC have not investigated the underlying mechanisms that cause stress relaxation, damage, and eventual rupture of composite samples. Hence, the focus of the present study is to push the limit of stress relaxation until failure and identify the mechanisms that lead to cracking or failure of ultra-thin composites under an imposed curvature. In general, the failure of HSC is stochastic in nature due to manufacturing imperfections and experimental procedure discrepancies. This work is aimed at eventually addressing these issues by utilizing micro computed tomography (μCT) imaging, using a micro-CT X-ray scanner available in our lab. New test designs which allow us to test several samples simultaneously while applying a constant curvature were considered for this purpose. In the first design referred to as Coiled to Rupture (CTR) test, the sample is placed over a rigid cylinder and is held in place by pressure. This test configuration allows the sample to be removed for imaging at regular time intervals, between the time when the sample was first deformed and up to the point of rupture. In this experiment, the time to failure of the samples is recorded for different stowage temperatures and applied curvatures. Because the samples are completely unloaded for imaging, the micro-structural changes are hard to observe until the sample finally ruptures. For this purpose, a second test design has been developed, which is referred to as Flattening to Rupture (FTR) test. This is advantageous for allowing in-situ imaging of the samples while in a loaded configuration.

Micro-structural observations are the key to identifying the mechanisms causing time-dependent failure. X-ray micro computed tomography (μCT) is ideal for this purpose as a non-destructive inspection technique where three-dimensional features of the micro-structure can be observed. Research on the use of X-ray μCT as a quantitative tool has been carried out [9]. Since μCT is a non-destructive technique, it is a most suitable candidate for analyzing micro-structural changes over time through time-lapse sequence of 3D volumes, also known as Temporal Computed Tomography [10].

The goal of this paper is to observe and quantify the time-dependent failure characteristics of ultra-thin ply fiber composites by observing their micro-structural changes. Section III explains the theoretical concepts behind the experimental setup. Section IV details the experimental procedure for the material relaxation phase and describes the material of interest. Sections V and VI present the results of the studies to evaluate the time to rupture and to measure permanent deformation accumulation over time. Difficulties faced during micro-structural observations and an alternative way to tackle these difficulties are explained in Section VII. Section VIII outlines work currently in progress and concludes the paper.

III. Theoretical Concepts

A. Constitutive relation of HSC

Due to the thinness and high shear stiffness of HSC, laminates can be modelled under the assumptions of classical lamination theory (CLT). The constitutive relation under CLT for non-viscoelastic shells expressed in Eq. (1). The ABD stiffness matrix defines the constitutive relationship between the in-plane forces (N_x, N_y, N_{xy}) and out-of plane moments (M_x, M_y, M_{xy}) with the mid-plane strains $(\epsilon_x^0, \epsilon_y^0, \epsilon_{xy}^0)$ and curvatures $(\kappa_x, \kappa_y, \kappa_{xy})$

$$\begin{bmatrix} N_x \\ N_y \\ N_{xy} \\ M_x \\ M_y \\ M_{xy} \end{bmatrix} = \begin{bmatrix} A_{11} & A_{12} & A_{16} & B_{11} & B_{12} & B_{16} \\ A_{21} & A_{22} & A_{26} & B_{21} & B_{22} & B_{26} \\ A_{61} & A_{62} & A_{66} & B_{61} & B_{62} & B_{66} \\ B_{11} & B_{21} & B_{16} & D_{11} & D_{12} & D_{16} \\ B_{12} & B_{22} & B_{62} & D_{21} & D_{22} & D_{26} \\ B_{16} & B_{26} & B_{66} & D_{61} & D_{26} & D_{66} \end{bmatrix} \begin{bmatrix} \epsilon_x^0 \\ \epsilon_y^0 \\ \epsilon_{xy}^0 \\ \kappa_x \\ \kappa_y \\ \kappa_{xy} \end{bmatrix} \tag{1}$$

The generalization of the above constitutive relation to viscoelastic laminates [11] using the Boltzmann superposition integral is as follows,

$$N_i(t) = \int_0^t \left(A_{ij}(t-\tau) \frac{\mathrm{d}\epsilon_j^0(\tau)}{\mathrm{d}\tau} + B_{ij}(t-\tau) \frac{\mathrm{d}\kappa_j(\tau)}{\mathrm{d}\tau} \right) \mathrm{d}\tau \tag{2}$$

$$M_i(t) = \int_0^t \left(B_{ij}(t-\tau) \frac{\mathrm{d}\epsilon_j^0(\tau)}{\mathrm{d}\tau} + D_{ij}(t-\tau) \frac{\mathrm{d}\kappa_j(\tau)}{\mathrm{d}\tau} \right) \mathrm{d}\tau \tag{3}$$

Under stowage conditions, the non-zero kinematic load $\kappa_x(t) = \kappa_0 H(t)$ is assumed, where κ_0 is the imposed curvature and $H(t)$ is the Heaviside function. All other mid-plane strains and curvatures are zero. For the symmetric layups considered in this study, axial and bending deformations are decoupled and hence $B_{ij} = 0$.

To impose this state of loading HSC coupons are bent over a rigid cylinder and kept in place by a normal pressure applied by a Kapton membrane. To maintain consistency between all the coupons, identical weights $W = 2\,\mathrm{kg}$ were used to apply the same pressure. Fig. 1 shows a schematic view of the test setup. This test setup is referred to as Coiling to Rupture (CTR) test. Since the coupons are kept in place only by the normal pressure $P = P(\theta)$, it can be assumed that no in-plane force resultants act on the coupons.

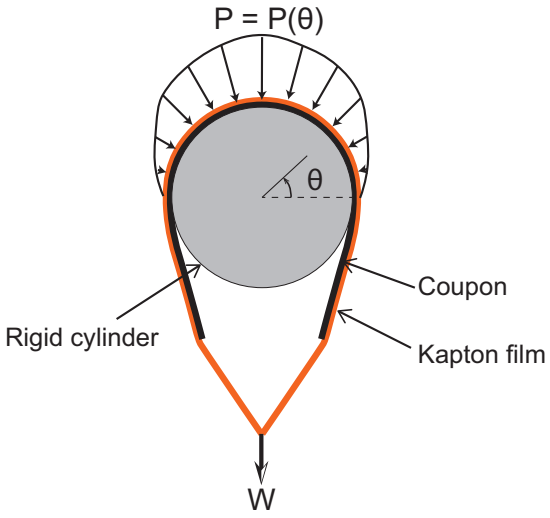

Fig. 1 Schematic of the test setup.

B. Time-temperature superposition

Generally, the viscoelastic properties of polymers are known to have time and temperature dependency. The time-dependent behavior tests are accelerated by combining time-temperature effects through a correction known as the time-shift factor a_T in the real time-scale t. The reduced time t' is related to the real time by

$$t' = \int_0^t \frac{\mathrm{d}\tau}{a_T(T)} \tag{4}$$

The class of materials having the same shift factor throughout all relaxation times are termed thermo-rheologically simple. The time-shift factor can be obtained using Arrhenius law for the temperature range below the glass-transition temperature of the polymer [12],

$$\ln(a_T) = -\frac{E_a}{\mathrm{R}}\left(\frac{1}{T} - \frac{1}{T_0}\right) \tag{5}$$

where E_a is the activation energy, R the universal gas constant, T the actual temperature and T_0 the reference temperature at which the material characterization tests are carried out.

Because the polymer constituent in composite materials is the main source of their time-dependent behavior, the time-temperature principle can be applied for carrying out accelerated testing at raised temperatures.

In this study, experiments are conducted to quantify and understand the underlying mechanisms causing stress relaxation and failure under long duration loads. In thin-ply composites, viscoelastic micro-damage can initiate in the matrix and the region of damage can grow steadily. Under a flexural load, as the micro-damage grows, it can lead to the formation of macroscopic cracks due to kinking in the compression region of the sample.

C. Preliminary observations

Observation of ruptured samples under an optical microscope and X-ray μCT imaging shows that the cracks appear near the compression surface of samples under flexure Fig. 2 (a). These observations suggests that compression type failure mechanisms such as micro-buckling of fibers lead to kinking. An approach to looking for evidence to support this conjecture is presented in the present paper.

The most common failure mode of fiber composites under compression is micro-buckling of the fibers, forming a kink band resisted by plastic deformation of the matrix [13, 14]. Analysis of kinking in aligned-fiber composites was first modeled by Rosen [15] considering elastic buckling of an axially compressed, perfectly aligned fibers and later extended by Argon [13] and Budiansky [16] considering effects of matrix yielding and fiber misalignment. The model proposed by Budiansky [16] for the critical compressive stress is expressed as,

$$\sigma_c = \frac{G}{1 + \frac{\phi_0}{\gamma_y}} \tag{6}$$

Where G is the shear modulus of the composite, ϕ_0 is the initial fiber misalignment and γ_y is the yield shear strain of the composite. The presence of a polymeric constituent in a fiber composite is the dominant factor for the time-dependent behavior of the composite. Time-dependent effects in the fiber are order of magnitudes smaller than in the matrix [17]. The modulus reduction over time and temperature, and hence the shear modulus of the composite, decays with time and can be approximated by the Prony series,

$$G(t) = G_\infty + \sum_{i=1}^{n}\left(G_i \mathrm{e}^{-\frac{t}{\tau_i}}\right) \tag{7}$$

where G_∞ is the long term modulus, G_i are the Prony coefficients and τ_i are the relaxation times. Each exponential term corresponds to the variation of the relaxation modulus over a time period. The number of terms included in the Prony series depends on the time scale of the problem of interest.

IV. Experimental Details

A. Manufacturing of Composite Samples

The HSC considered for the present study consisted of plain weave glass fiber (PWGF) and uni-directional carbon fiber (UDCF) layers. The PWGF plies are 25 grams per square meter (gsm) glass fibers, with NTPT ThinPreg 402T

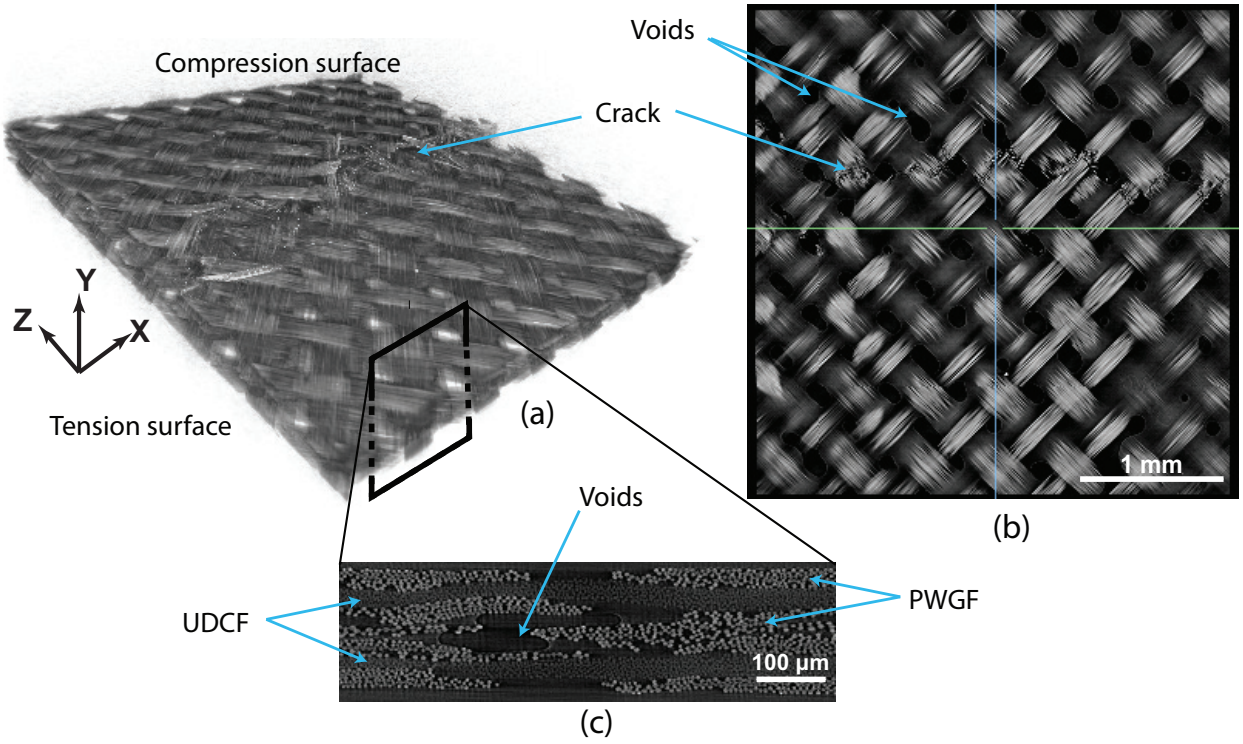

Fig. 2 (a) 3D view of X-Ray μCT image of the ruptured sample, (b) XZ plane view of the compression surface and (c) high resolution image of XY plane.

epoxy resin, while the UDCF plies are made of 30 gsm MR70 fibers, with NTPT ThinPreg 402T epoxy resin. The laminate consisted of a single ±45 PWGF ply, sandwiched between two, 3-ply prepreg tape of [±45 PWGF /0 UDCF/±45 PWGF] supplied by North Thin Ply Technology. 7-ply laminates were prepared from the prepregs and cured in an autoclave using vacuum bagging with a flat aluminum plate on one side. This particular laminate is of interest because it is used in the coilable longerons for the Space Solar Power Project (SSPP) at Caltech, discussed in [18]. This 7-ply laminate corresponds to the web-section of the longerons for the SSPP structure.

The test coupons were cut from 180 mm × 80 mm flat panels using a laser cutter. The coupons were 20 mm wide and 90 mm long with 2 mm wide and 2 mm deep triangular notches along each side, as shown in Fig. 3. These notches acts as a stress concentrator to trigger rupture at a known location.

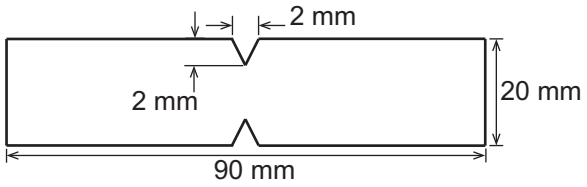

Fig. 3 Schematic of HSC test coupon.

B. Micro-Computerized Tomography (µCT) imaging

A ZEISS Xradia 510 Versa 3D X-ray microscope (XRM) was used to produce μCT images of the micro-structure of the test samples. This system is capable of producing images at a wide range of magnifications, ranging from 0.7 μm true spatial resolution with a voxel size of 70 nm to mm scale resolution. This allows imaging of the samples across different length scales. The μCT image of a composite sample shown in Figs. 2(a) and 2(b) has a voxel size of 4 µm and the field of view is 4 mm × 4 mm × 4 mm. This image was obtained with a 40 kV voltage setting and an exposure time

of 3 s per projection. The 3D volume was reconstructed with 3001 projections. Fig. 2(c) shows a high resolution μCT image obtained with a voxel size of 0.7 µm and the field of view is 0.7 mm × 0.7 mm × 0.7 mm. Analysis of this image shows the asymmetric nature of warp and weft tows of the PWGF layer. In addition, significant voids are seen inside the sample. During relaxation phase of the test sample, presence of the voids may play a significant role in damage initiation, as void growth may trigger delamination and fiber micro-buckling.

C. Experimental setup of Coiling to Rupture (CTR) test

An experimental setup was developed to impose a constant curvature, to replicate the conditions under what stress relaxation takes place during stowage. A rigid cylinder was used to impose a constant curvature on the test samples. The setup used for the test is shown in Fig. 4. The samples were placed over the rigid cylinder and then covered with a Kapton membrane. Weights were hung to the Kapton membrane in order to ensure the samples conform to the cylinder. Cylinders with four different radii were used: $R = \{4\,\text{mm},\ 4.25\,\text{mm},\ 4.5\,\text{mm}$ and $4.75\,\text{mm}\}$ corresponding to the curvatures $\kappa_0 = \{0.250\,\text{mm}^{-1},\ 0.235\,\text{mm}^{-1},\ 0.222\,\text{mm}^{-1}$ and $0.210\,\text{mm}^{-1}\}$ respectively. These curvature values are chosen close to the instantaneous failure curvature ($0.24 \pm 0.003\ \text{mm}^{-1}$) determined from the Column Bending Test [8]. The test setup shown in Fig. 4(a) was then placed in an oven at a temperature of 70^oC and 90^oC for accelerated relaxation testing.

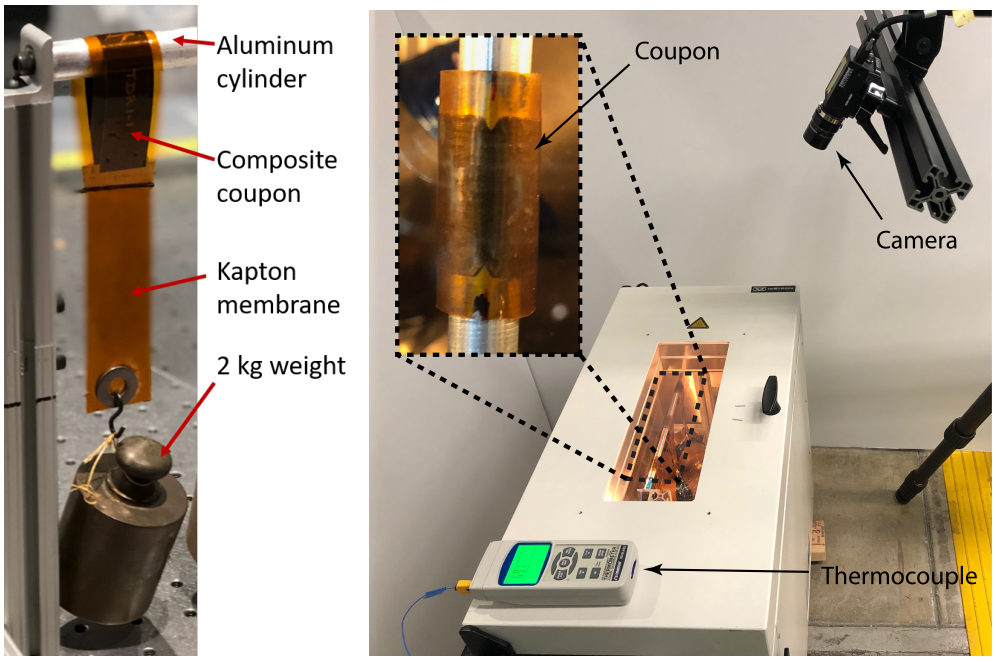

Fig. 4 Experimental setup.

Once the relaxation phase had been reproduced in this simple experimental setup, the time scale damage evolution/ micro-structural changes over given relaxation times was studied. The variables considered in the following studies are: imposed curvature κ_0, relaxation temperature T_{relax} and relaxation time t_{relax}. The time for rupture was observed using a video camera outside the oven. When the coupon failed the uniform curvature region deformed into a kinked shape. By observing the images taken from the camera the exact time of rupture was measured. The process was accelerated by carrying out tests at two different temperatures 70^oC and 90^oC. These temperatures are well below the curing temperature (125^oC) and the glass-transition temperature 185^oC as per data-sheet. Once the curvature had been imposed using the setup shown in Fig. 4, the entire setup was placed inside an oven and the temperature was increased from room temperature to the desired temperature at a rate of 2^oC per minute. The local temperature near the coupons was measured using two thermocouples. The temperature used only as an accelerator of the process and the trends under different temperature was observed. Based on the time-temperature superposition theory, it is expected that in the process accelerated using higher temperatures the time to rupture will be shorter.

V. Time to Rupture Study

Using the CTR test setup shown in Fig. 4(b) tests were conducted until the samples failed by cracking on the compression surface in order to quantify the time to rupture under different curvatures and temperatures. Fig. 5 shows the collected data of samples from the tests carried out for each imposed curvature and for each temperature. The temperature ramp time is shown by the grey area in the plot. Test coupons that did not show any damage within 5 days are reported as "Not Failed" in the plot. The normalized curvature ($\hat{\kappa}$) is the ratio between the imposed curvature (κ_0) and the instantaneous failure curvature (κ_f) of the laminate.

The instantaneous failure curvature was determined to be 0.24 $\pm$0.003 mm^{-1} using the Column Bending Test approach [8]. Obviously, curvature ratios greater than 1 correspond to instantaneous failures. Note that five data points correspond to a normalized curvature of 1.04. This curvature value is greater than the instantaneous failure curvature. Hence, regardless of the temperature these test samples failed instantaneously. Both arithmetic mean and geometric mean of the measured times to rupture were calculated for each imposed curvature and temperature. Note that measurements within the temperature ramp region were discarded from the mean failure time calculation. It is suspected that premature failure in this range may be due to the effects of thermal gradients while heating as well as uncertainty due to manufacturing defects of material. Both means are presented in Table 1 for comparison.

Note that the data has a scatter ranging several orders of magnitude. Since the geometric mean can be interpreted as the arithmetic mean of the log quantities,

$$\text{Geometric mean} = \sqrt[n]{\prod t_i} = \exp\left(\frac{1}{n}\sum \ln(t_i)\right) \tag{8}$$

and the underlying reason for the time-dependent failure is the strength reduction over time, which is an exponential decay as expressed in Eq. (7), taking the geometric mean is more appropriate in this case.

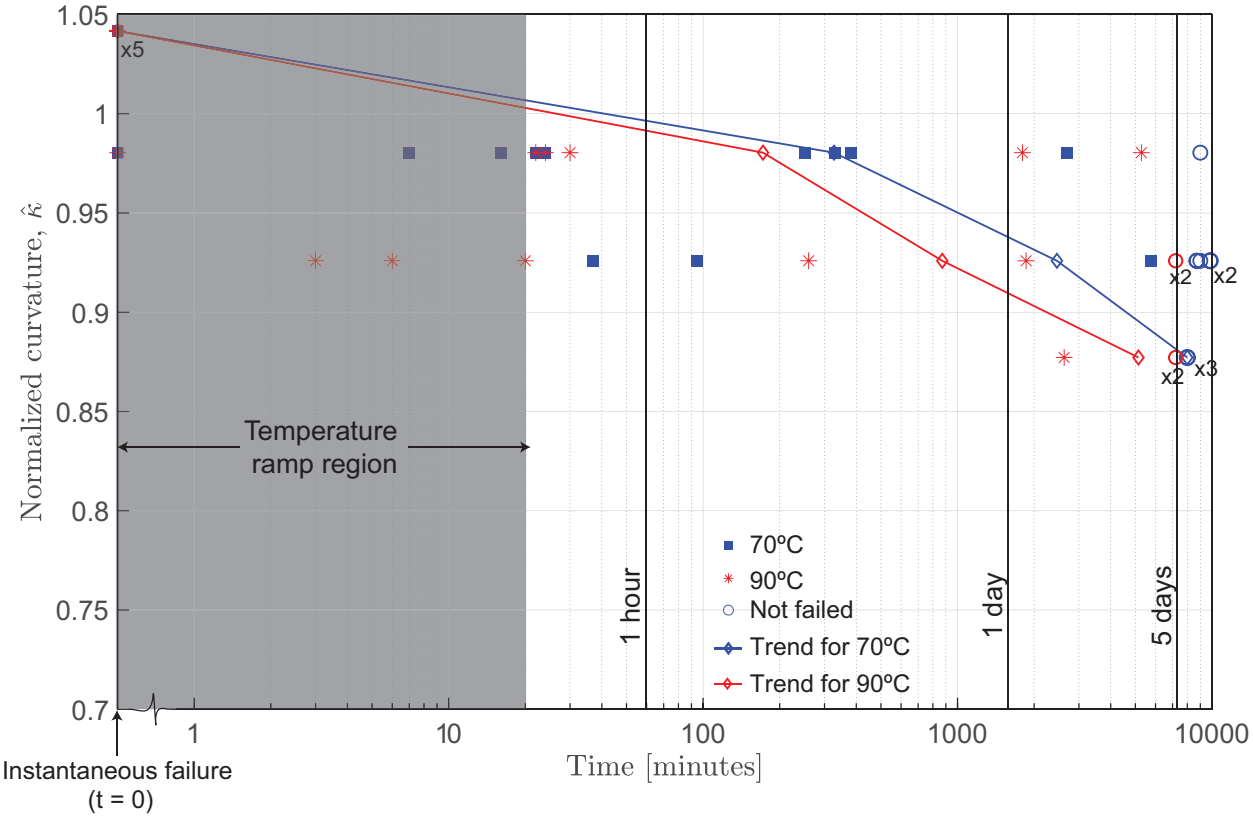

Fig. 5 Time to rupture.

Table 1 Comparison of arithmetic and geometric means.

Normalized curvature	Time to rupture at 70^oC in minutes		Time to rupture at 90^oC in minutes	
$\hat{\kappa} = \kappa_0/\kappa_f$	Arithmetic mean	Geometric mean	Arithmetic mean	Geometric mean
0.98	1813	327	1431	172
0.93	6497	2459	3308	871
0.88	8000	8000	5675	5143

VI. Permanent deformation accumulation / curvature recovery study

Thin composites exhibit damage accumulation over long-term imposed curvatures. An attempt was made to correlate the damage accumulation with the residual deformation after chosen relaxation times. It was observed that the coupons exhibit residual curvature when removed from the setup after a set relaxation time and part of the curvature is recovered over time.

From the time to rupture study the damage accumulation region was identified and for this study an imposed curvature of 0.222 mm^{-1} was chosen to understand and quantify the residual deformation after relaxation times of 2, 4, 6 hours until failure. The relaxation tests were conducted by utilizing the CTR test setup shown in Fig. 4 and placed in the oven at 70^oC. The coupon was relaxed for 2 hours and then removed from the setup. The coupon was allowed to recover the curvature at room temperature, as shown in Fig. 6. The curvature of the coupon was measured using the VIC-3D Digital Image Correlation setup continuously over 5 days. After this test the coupons were placed again in the oven for the next relaxation of 2 additional hours, using the experimental setup. This process was repeated until failure.

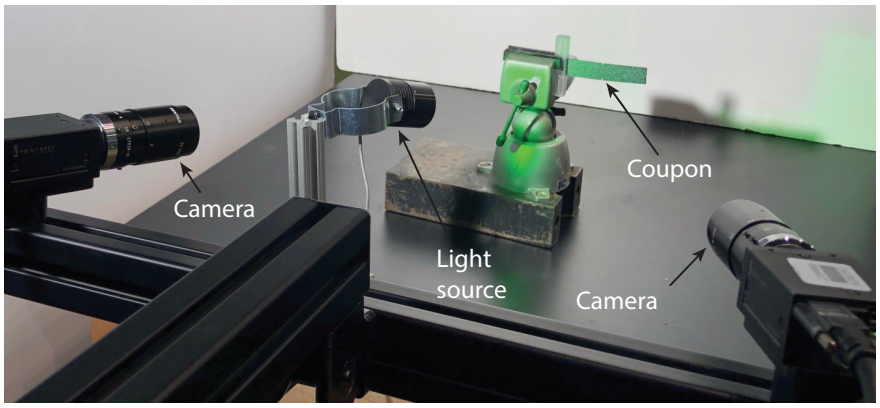

Fig. 6 Curvature recovery test setup.

Fig. 7 shows the results obtained for a coupon tested in this way. The difference between the current longitudinal curvature and the initial longitudinal curvature of the sample (after manufacturing) has been plotted against time. $\Delta\kappa_1^e$, $\Delta\kappa_2^e$ and $\Delta\kappa_3^e$ are corresponding to the elastic recovery and $\Delta\kappa_1^p$, $\Delta\kappa_2^p$ and $\Delta\kappa_3^p$ are corresponding to the residual curvature of the test coupons after relaxation times of 2, 4 and 6 hours respectively. Note that the residual curvatures increased monotonically during the test. The recovered portion is due to the viscoelastic nature of the composite and the residual curvature is corresponds to the damage accumulation or viscoplastic behavior. An increase in the residual curvature was observed for an increase in the relaxation period.

VII. Micro-Structural Observation Study

The mechanisms leading to time-dependent rupture were studied. The X-ray μCT scanner was used to observed the micro-structure of ruptured coupons, at the end of the tests presented in section V. Fig. 8 shows evidence for the failure mechanisms observed in a coupon ruptured after 260 minutes at an imposed curvature of 0.222 mm^{-1} at 90^oC. The dominant failure mechanisms are micro-buckling and delamination. The YZ cross sectional view shown by the orange bounding box shows the delamination between the uni-directional carbon fiber (UDCF) layer and the plain-weave glass fiber (PWGF) layer on the compression side of the coupon. The delamination region is denoted by red dashed lines.

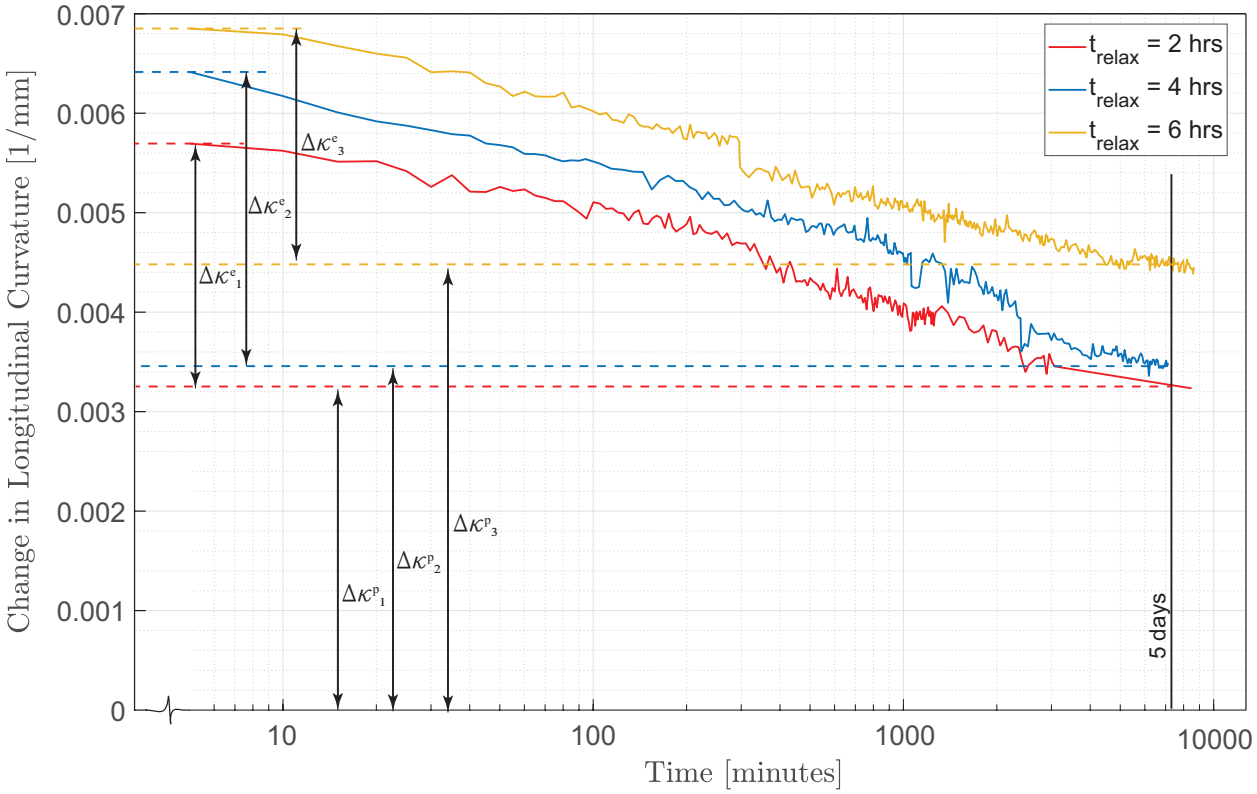

Fig. 7 Curvature recovery plot.

The XZ cross sectional view shown by a blue bounding box shows fiber breakage in the tows of the PWGF and the UDCF. In the XY sectional view shown by the green bounding box is the PWGF layer above the bonding layer. Here the kink band is clearly identified.

Coupons were tested using the CTR test setup described in section IV.C and removed for μCT imaging after a certain amount of relaxation. It is important to image the same part of the coupon, to compare the micro-structural changes. Since the notches in the coupon serve to localize the rupture, the notches were also used as a location reference for the μCT imaging. μCT images were obtained with 4 µm voxel size resulting in a 4 mm $\times$ 4 mm $\times$ 4 mm volume. However, no significant micro-structural changes were observed and it was conjectured that the damage feature detectability may have been decreased by the unloaded condition in which the samples were imaged. The micro-buckled fibers may have recovered and small delaminations and cracks may have closed during unloading. Several approaches to increase the detectability of damage were investigated and it was decided to image the test coupons in a loaded configuration. Using the current experimental setup, additional fixtures would be needed to keep the coupons curved and these fixtures would interact with the path of the X-ray and adversely affect the image quality, increasing the scan time depending on the thickness of the fixtures.

Instead, it was decided to manufacture initially curved samples and to impose curvature changes by flattening the samples. The resulting experimental setup is referred to as Flattening to Rupture (FTR) test. Hence, during the relaxation phase at elevated temperatures the samples would be kept in a flattened configuration. μCT images of the flat samples would be taken, allowing us to image them in a loaded configuration. The underlying assumption here is that micro-structural changes are insignificant at room temperature compared to the elevated temperatures of 70^{o}C and 90^{o}C at which the relaxation phase of the test has been carried out. Therefore, it is assumed that imaging time does not count towards the total time during which the sample has been kept flat.

A 7-ply laminate was prepared using an aluminum mold with a narrow curved region in the middle and two tangent flat regions on either side as shown in Fig. 10(a). The narrow curved region defines the area where the cracks will initiate and it helps us to locate the field of view for the time-series μCT images. Coupons are 20 mm wide, 75 mm long and the arc length of the curved region is 5 mm. Flattening of the curved sample is achieved by sandwiching it between two glass plates and clamping them at the edges as shown in Fig. 9(a). In addition to the above stated advantage, another

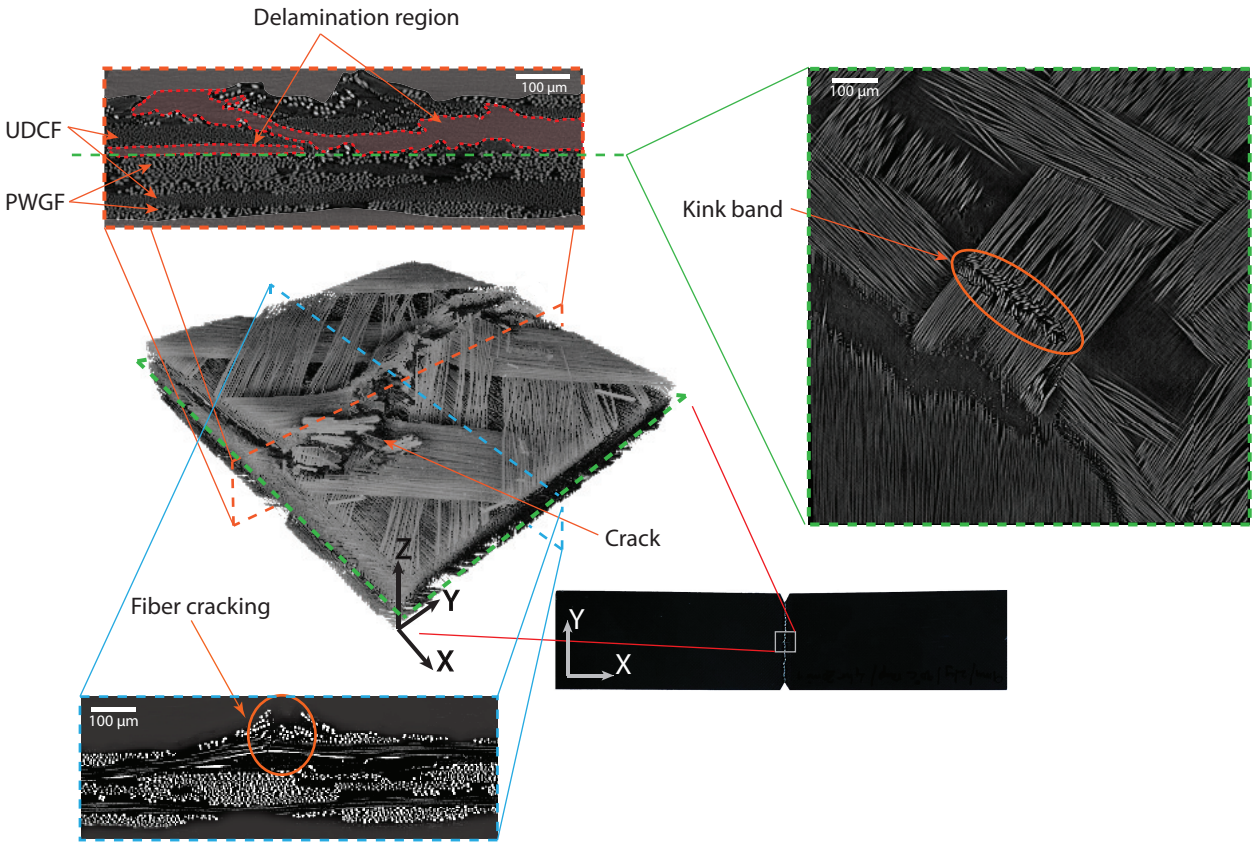

Fig. 8 μCT image of a ruptured sample.

important benefit from this approach is the possibility of observing the compression surface during relaxation and to precisely quantify the time for the first crack to appear. From the previous method it was only possible to determine the time taken for the complete rupture because the compression surface is not visible. Fig. 9(b) shows the evolution of a crack over time on the compression surface of the flattened coupon. Initially a surface crack initiated at t = 570 s and propagated. Later, at t = 948 s, another crack initiated and started to propagate. This opens up the possibility to study the crack propagation behavior.

VIII. Conclusion and Work in Progress

In this study, two new experimental setups for long-term relaxation testing of HSC laminates under applied curvature changes have been presented. In the CTR experimental setup, the samples were placed over a rigid cylinder, and held in place using pressure load, which impose a state of constant curvature in the samples. Using the CTR test setup, data was obtained for time to rupture, which showed a large scatter in the results. This is attributed to material imperfections in the manufactured samples. In addition, curvature recovery measurements were made after removing a loaded sample from the CTR test at regular time intervals. There is a need for more curvature recovery experiments to conclude the nature of the trend of damage accumulation and the threshold of the residual curvature without failure. To better understand the micro-structural changes that lead to rupture, the FTR experimental setup has been proposed. In the FTR test, the initially curved test samples are flattened using two glass plates, which impose a constant curvature change. This provides a transparent view for the damage growth in the sample during the test. An additional advantage of the FTR test is that in-situ μCT imaging is made possible, where a HSC sample can be scanned at regular time intervals for analyzing changes in the micro-structure in loaded configuration. Results from the new FTR experimental setup will be presented in future publications.

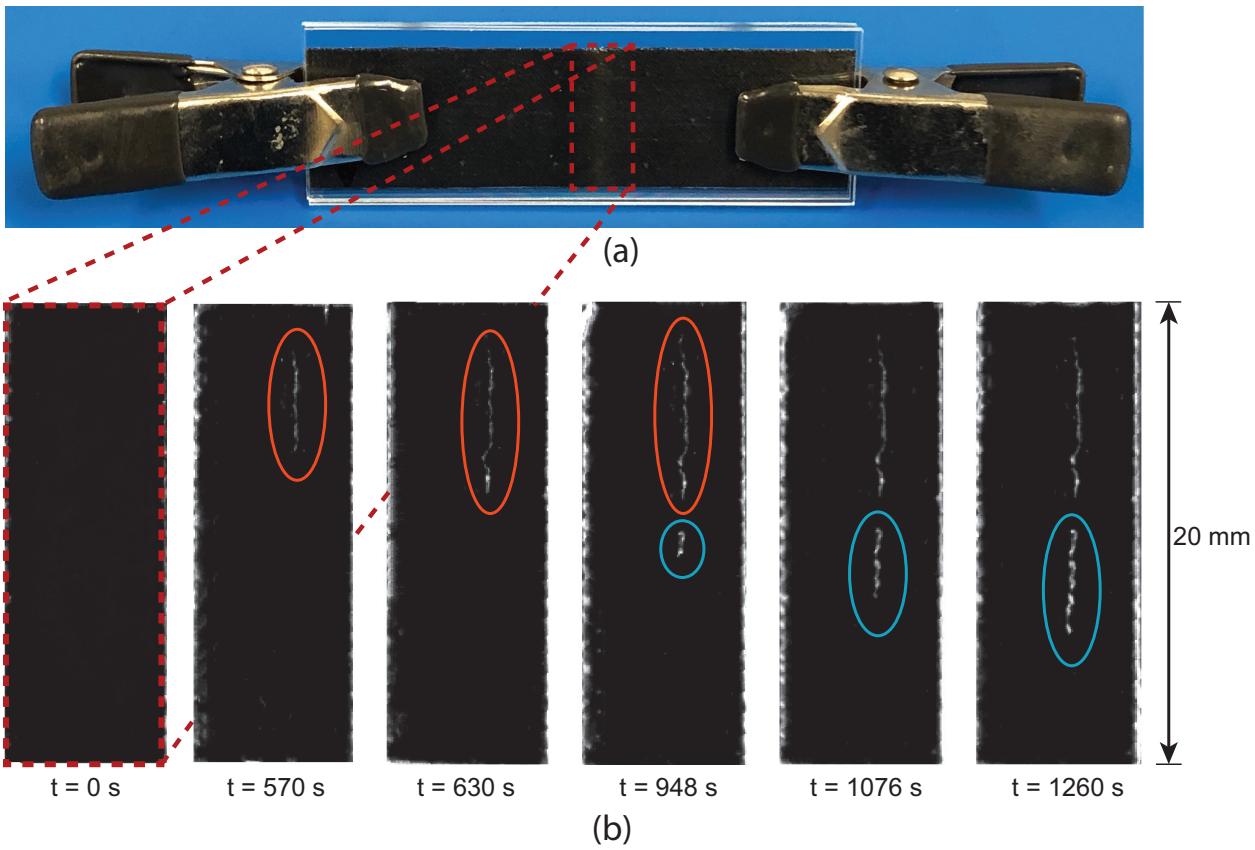

Fig. 9 (a) Flattening of initially curved coupons and (b) crack evolution of a curved sample.

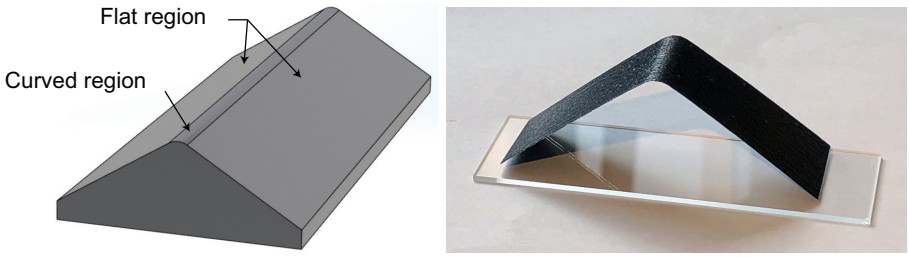

Fig. 10 (a) Mold used for manufacturing, (b) curved coupon.

Acknowledgments

The authors acknowledge financial support from the Space Solar Power Project at Caltech. In addition, we would like to thank Alan Truong for helping us with manufacturing of HSC for this study.

References

[1] Banik, J., Kiefer, S., LaPointe, M., and LaCorte, P., "On-orbit validation of the roll-out solar array," *2018 IEEE Aerospace Conference*, IEEE, 2018, pp. 1–9.

[2] Arya, M., Lee, N., and Pellegrino, S., "Ultralight structures for space solar power satellites," *3rd AIAA Spacecraft Structures Conference*, 2016, p. 1950.

[3] Kwok, K., and Pellegrino, S., "Viscoelastic effects in tape-springs," *52nd AIAA/ASME/ASCE/AHS/ASC Structures, Structural Dynamics and Materials Conference 19th AIAA/ASME/AHS Adaptive Structures Conference 13t*, 2011, p. 2022.

[4] Kwok, K., and Pellegrino, S., "Micromechanical modeling of deployment and shape recovery of thin-walled viscoelastic composite space structures," *53rd AIAA/ASME/ASCE/AHS/ASC Structures, Structural Dynamics and Materials Conference 20th AIAA/ASME/AHS Adaptive Structures Conference 14th AIAA*, 2012, p. 1910.

[5] Brinkmeyer, A., Pellegrino, S., and Weaver, P. M., "Effects of long-term stowage on the deployment of bistable tape springs," *Journal of Applied Mechanics*, Vol. 83, No. 1, 2016, p. 011008.

[6] Rose, T. J., Medina, K., Francis, W., Kwok, K., Bergan, A., and Fernandez, J. M., "Viscoelastic Behavior of High Strain Composites," *AIAA/ASME/ASCE/AHS/ASC High-Strain Composite Materials and Structures II*, 2019.

[7] Medina, K., Rose, T., and Fransis, W., "Long-term Stress Rupture Limitations of Unidirectionasl High Strain Composites in Bending," *Proceedings of the American Society for Composites—Thirty-third Technical Conference*, 2018.

[8] Fernandez, J. M., and Murphey, T. W., "A Simple Test Method for Large Deformation Bending of Thin High Strain Composite Flexures," *2018 AIAA Spacecraft Structures Conference*, 2018, p. 0942.

[9] Maire, E., and Withers, P. J., "Quantitative X-ray tomography," *International materials reviews*, Vol. 59, No. 1, 2014, pp. 1–43.

[10] Garcea, S., Wang, Y., and Withers, P., "X-ray computed tomography of polymer composites," *Composites Science and Technology*, Vol. 156, 2018, pp. 305–319.

[11] Kwok, K., and Pellegrino, S., "Micromechanics models for viscoelastic plain-weave composite tape springs," *AIAA Journal*, Vol. 55, No. 1, 2016, pp. 309–321.

[12] Brinson, H. F., and Brinson, L. C., *Polymer engineering science and viscoelasticity*, Springer, 2015.

[13] Argon, A., "Fracture of Composites," *Treatise on Materials Science & Technology*, Vol. 1, Elsevier, 1972, pp. 79–114.

[14] Budiansky, B., and Fleck, N. A., "Compressive kinking of fiber composites: a topical review," 1994.

[15] Rosen, B. W., "Mechanics of composite strengthening." 1965.

[16] Budiansky, B., "Micromechanics," *Computers & Structures*, Vol. 16, No. 1-4, 1983, pp. 3–12.

[17] Sullivan, J., "Creep and physical aging of composites," *Composites Science and Technology*, Vol. 39, No. 3, 1990, pp. 207–232.

[18] Leclerc, C., and Pellegrino, S., "Reducing Stress Concentration in the Transition Region of Coilable Ultra-Thin-Shell Booms," *AIAA Scitech 2019 Forum*, 2019, p. 1522.